

Supporting Information

Size/Morphology Induced Tunable Luminescence in Upconversion Crystals: Ultra-Strong Single-Band Emission and Underlying Mechanisms

*Zhaofeng Wang,^a Songshan Zeng,^a Jingfang Yu,^a Xiaoming Ji,^b Huidan Zeng,^b Shuangyu Xin,^c
Yuhua Wang^c and Luyi Sun^{*a}*

*^aDepartment of Chemical & Biomolecular Engineering and Polymer Program, Institute of
Materials Science, University of Connecticut, Storrs, Connecticut 06269, United States*

*^bKey Laboratory for Ultrafine Materials of Ministry of Education, School of Materials Science
and Engineering, East China University of Science and Technology, Shanghai 200237, China*

*^cDepartment of Materials Science, School of Physical Science and Technology, Lanzhou
University, Lanzhou, 730000, China*

*Author to whom correspondence should be addressed:

Dr. Luyi Sun, Tel: (860) 486-6895; Fax: (860) 486-4745; Email: luyi.sun@uconn.edu

1. Crystal structure analysis

Crystal structures of all obtained Er^{3+} , Yb^{3+} co-doped lutetium oxyfluorides were identified by x-ray diffraction (XRD) as shown in Figure S1. All diffraction peaks agree well with the orthorhombic $\text{Lu}_n\text{O}_{n-1}\text{F}_{n+2}$ phase, without any detectable impurities. To further determine the value of n , the structure refinements of the patterns were carried out using the orthorhombic crystal system. Employing the sample synthesized at the condition of $\text{pH} = 1.5$, $C_{\text{NH}_4\text{F}} = 1.0 \text{ M}$ for example (Figure S2), after refinement, the cell parameters of the sample are obtained as $a = 5.4222 \text{ \AA}$, $b = 27.6026 \text{ \AA}$, $c = 5.5308 \text{ \AA}$. For orthorhombic crystal system, the cell parameters of a and c are always similar, while b can be expressed to be around $n \times 5.447 \text{ \AA}$.^{1,2} Therefore, the value of n is calculated to be 5, and the exact crystal phase of the final product is determined to be $\text{Lu}_5\text{O}_4\text{F}_7$.

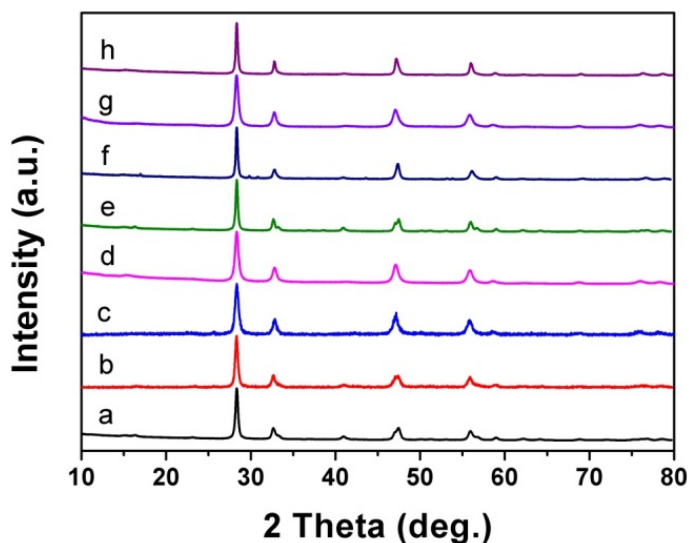


Figure S1. XRD patterns of Er^{3+} , Yb^{3+} co-doped lutetium oxyfluoride products prepared under different conditions. (a) $\text{pH} = 2.5$, $C_{\text{NH}_4\text{F}} = 0.5 \text{ M}$. (b) $\text{pH} = 2.5$, $C_{\text{NH}_4\text{F}} = 1.0 \text{ M}$. (c) $\text{pH} = 2.5$, $C_{\text{NH}_4\text{F}} = 2.0 \text{ M}$. (d) $\text{pH} = 1.5$, $C_{\text{NH}_4\text{F}} = 2.0 \text{ M}$. (e) $\text{pH} = 3.5$, $C_{\text{NH}_4\text{F}} = 2.0 \text{ M}$. (f) $\text{pH} = 5$, $C_{\text{NH}_4\text{F}} =$

2.0 M. (g) pH = 1.5, $C_{NH_4F} = 1.0$ M. (h) pH = 3.5, $C_{NH_4F} = 1.0$ M.

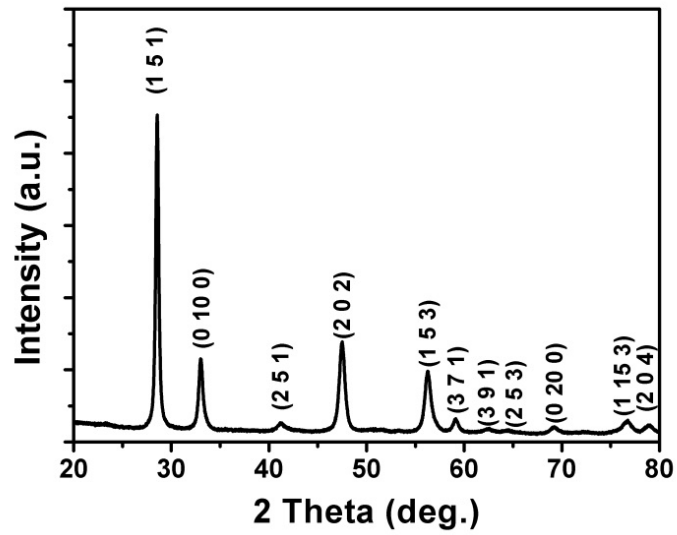


Figure S2. XRD pattern of $Lu_5O_4F_7: 0.5\%Er^{3+}, 20\%Yb^{3+}$ synthesized under the condition of pH = 1.5, $C_{NH_4F} = 1.0$ M.

2. UV-Vis-NIR absorption spectra

Figure S3 shows the UV-Vis-NIR absorption spectra of $\text{Lu}_5\text{O}_4\text{F}_7: 0.5\%\text{Er}^{3+}, 20\%\text{Yb}^{3+}$ products with different morphologies. The characteristic peaks of Er^{3+} are observed at 387, 521, and 669 nm, corresponding to the electron transfers of $^4\text{I}_{15/2} \rightarrow ^4\text{G}_{11/2}$, $^4\text{I}_{15/2} \rightarrow ^2\text{H}_{11/2}$, and $^4\text{I}_{15/2} \rightarrow ^4\text{F}_{9/2}$, respectively.³ Meanwhile, the broad absorption band in the region of 880-1200 nm with a sharp peak at ~ 975 nm can be ascribed to the characteristic $^2\text{F}_{7/2} \rightarrow ^2\text{F}_{5/2}$ transition of Yb^{3+} . The full-width at half-maximum (FWHM) is estimated to be ~ 80 nm, suggesting Yb^{3+} could be efficiently pumped by 975 nm laser and act as a good sensitizer in $\text{Lu}_5\text{O}_4\text{F}_7: \text{Er}^{3+}, \text{Yb}^{3+}$ crystals. The strong absorption from 200 to 280 nm could be ascribed to the host of $\text{Lu}_5\text{O}_4\text{F}_7$, in which slight blue-shifts (from 220 to 210 nm) were observed for the nanoparticles and nanorods due to quantum confinement effect.⁴

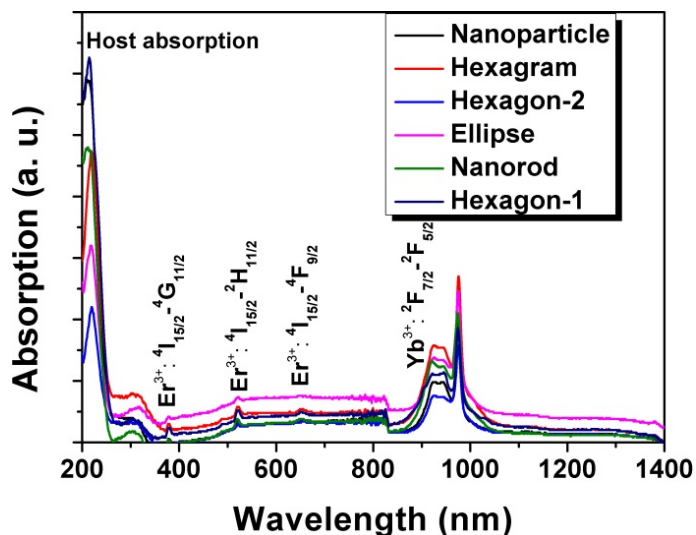


Figure S3. UV-Vis-NIR absorption spectra of the as-prepared $\text{Lu}_5\text{O}_4\text{F}_7: 0.5\%\text{Er}^{3+}, 20\%\text{Yb}^{3+}$ with different morphologies.

3. SEM images

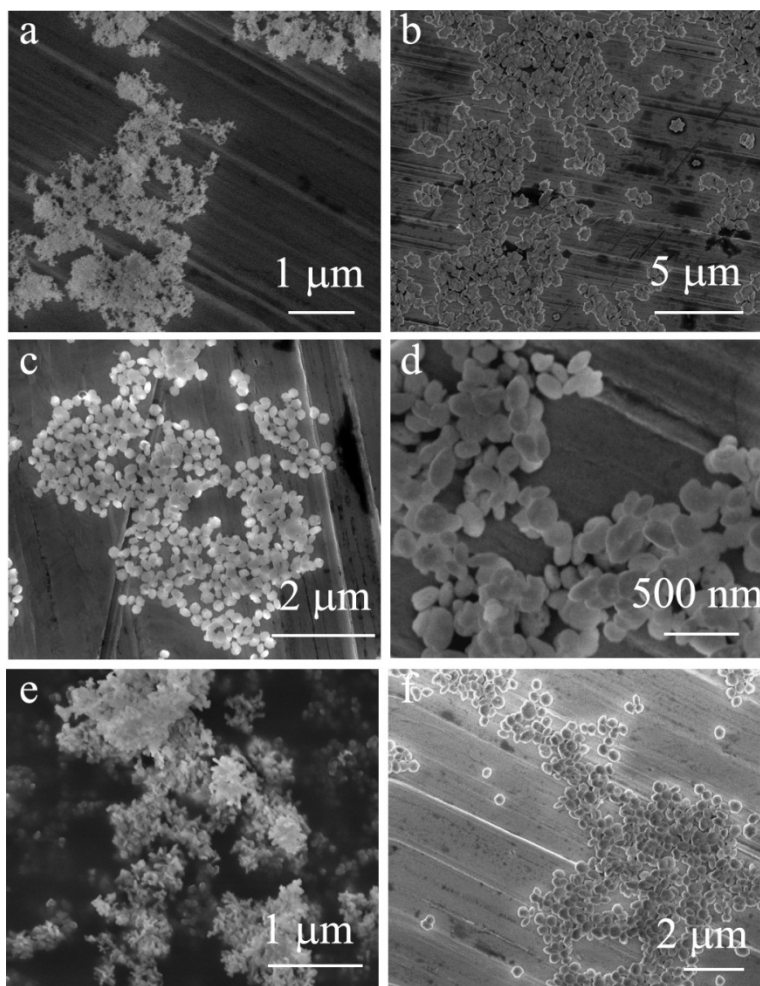


Figure S4. Representative low magnification SEM micrographs of $\text{Lu}_5\text{O}_4\text{F}_7:\text{Er}^{3+}, \text{Yb}^{3+}$ samples synthesized under different conditions. (a) $\text{pH} = 2.5, C_{\text{NH}_4\text{F}} = 0.5 \text{ M}$. (b) $\text{pH} = 2.5, C_{\text{NH}_4\text{F}} = 1.0 \text{ M}$. (c) $\text{pH} = 2.5, C_{\text{NH}_4\text{F}} = 2.0 \text{ M}$. (d) $\text{pH} = 1.5, C_{\text{NH}_4\text{F}} = 2.0 \text{ M}$. (e) $\text{pH} = 3.5, C_{\text{NH}_4\text{F}} = 2.0 \text{ M}$. (f) $\text{pH} = 1.5, C_{\text{NH}_4\text{F}} = 1.0 \text{ M}$.

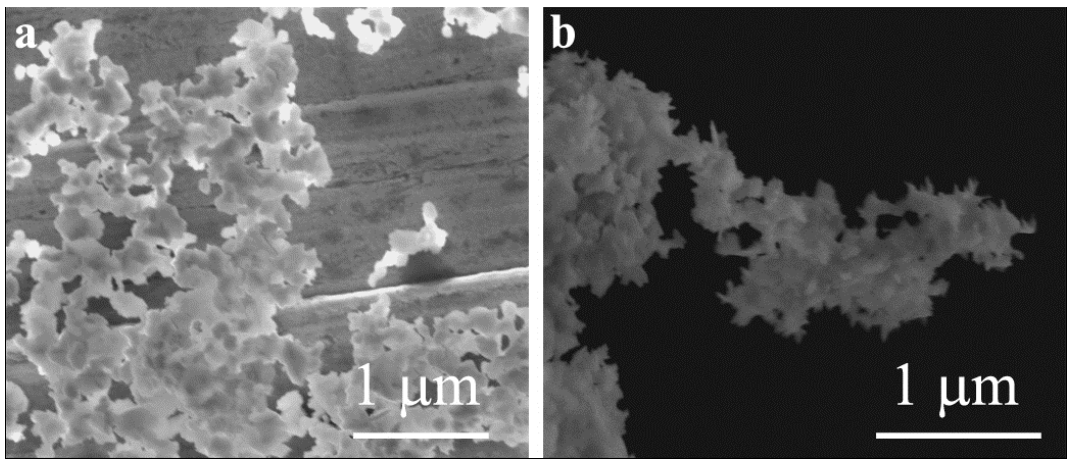


Figure S5. SEM micrographs of $\text{Lu}_5\text{O}_4\text{F}_7: 0.5\%\text{Er}^{3+}, 20\%\text{Yb}^{3+}$ samples with irregular morphology synthesized at (a) $\text{pH} = 5.0, C_{\text{NH}_4\text{F}} = 2.0 \text{ M}$ (irregular-1) and (b) $\text{pH} = 3.5, C_{\text{NH}_4\text{F}} = 1.0 \text{ M}$ (irregular-2).

4. Surface micro-structure investigation

The surface of the particles with morphology of hexagram, hexagon-1, hexagon-2 and ellipse appears to be rough. We investigated their TEM (Figure S6) and SEM (Figure S7) images under higher magnifications, considering that surface micro-structures are significant to the upconversion luminescence. For hexagram and hexagon-1, nanoparticles are tightly coated on the surface. However, porous structure is observed for the samples with the morphology of hexagon-2 and ellipse (The “smooth” surface in the top right of Figure S7b is aroused by the aggregation of charge when taking photos). The two different surface structures should be responsible for the two different upconversion features as described in the manuscript.

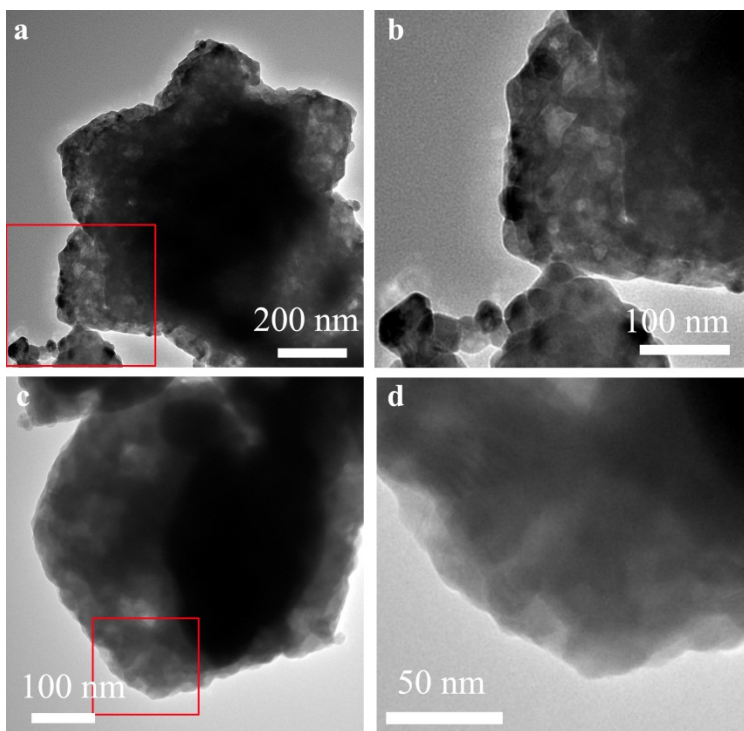


Figure S6. TEM micrographs of $\text{Lu}_5\text{O}_4\text{F}_7: 0.5\%\text{Er}^{3+}, 20\%\text{Yb}^{3+}$ (a,b) hexagram and (c,d) hexagon-1. (b) and (d) are the magnified images in the red regions in (a) and (c), respectively.

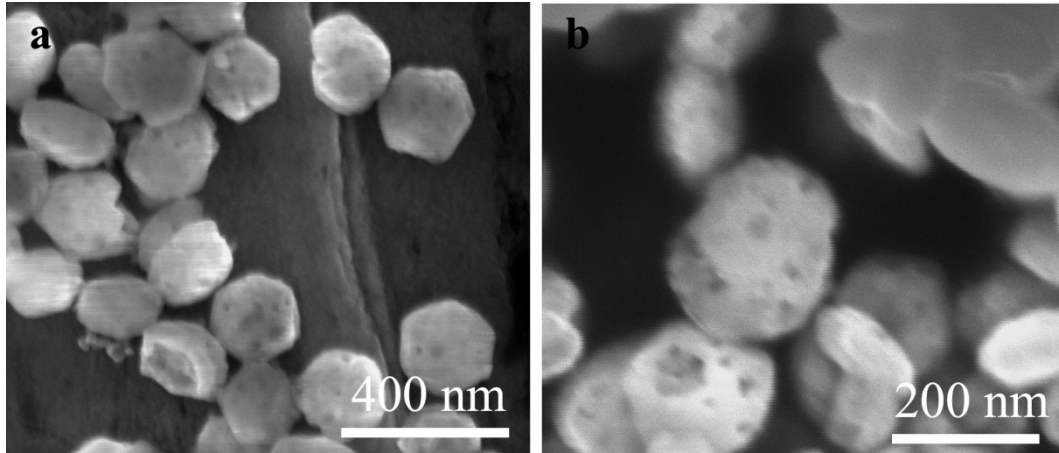


Figure S7. SEM micrographs of $\text{Lu}_5\text{O}_4\text{F}_7: 0.5\%\text{Er}^{3+}, 20\%\text{Yb}^{3+}$ (a) hexagon-2 and (b) ellipse.

5. Morphology and upconversion properties of NaYF₄: Er³⁺, Yb³⁺

For comparison, β -NaYF₄: Er³⁺, Yb³⁺ hexagonal prism was prepared, which was reported to exhibit strong upconversion emission.⁵ The SEM micrographs and XRD patterns of the prepared β -NaYF₄: Er³⁺, Yb³⁺ micro-crystals are presented in Figure S8, from which uniform β -NaYF₄: Er³⁺, Yb³⁺ hexagonal prisms with a length of $\sim 6 \mu\text{m}$ and a diameter of $\sim 1.2 \mu\text{m}$ can be clearly observed.

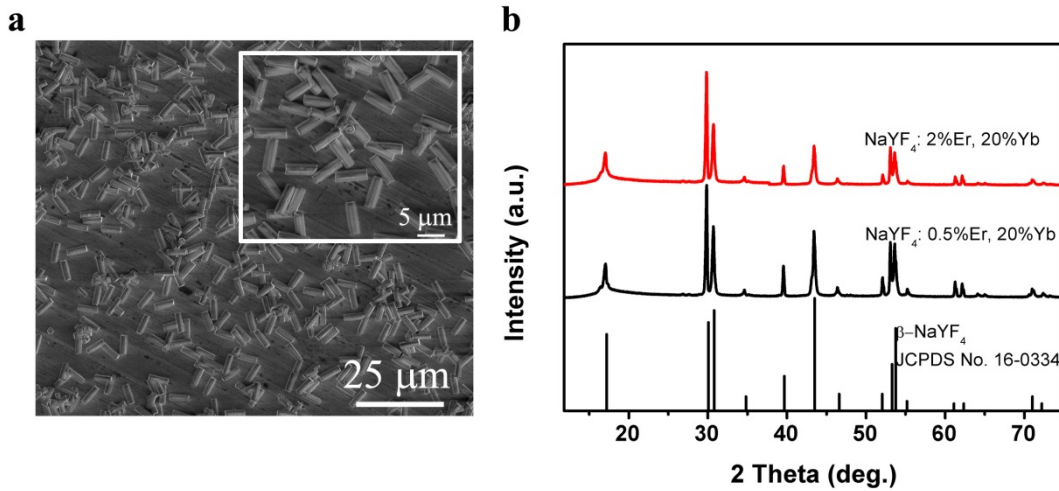


Figure S8. SEM images (a) and XRD patterns (b) of the prepared NaYF₄: Er³⁺, Yb³⁺ micro-crystals for the comparison of UC emission.

The upconversion spectra of β -NaYF₄: Er³⁺, Yb³⁺ hexagonal prisms on dependence of pump power are shown in Figure S9. Both β -NaYF₄: Er³⁺, Yb³⁺ samples with two kinds of doping concentrations (0.5% Er³⁺, 20% Yb³⁺ and 2% Er³⁺, 20% Yb³⁺) exhibit green emissions at 521 and 554 nm, red emission at 653 nm, corresponding to the $^2\text{H}_{11/2} \rightarrow ^4\text{I}_{15/2}$, $^4\text{S}_{3/2} \rightarrow ^4\text{I}_{15/2}$ and $^4\text{F}_{9/2} \rightarrow ^4\text{I}_{15/2}$ transitions of Er³⁺, respectively.

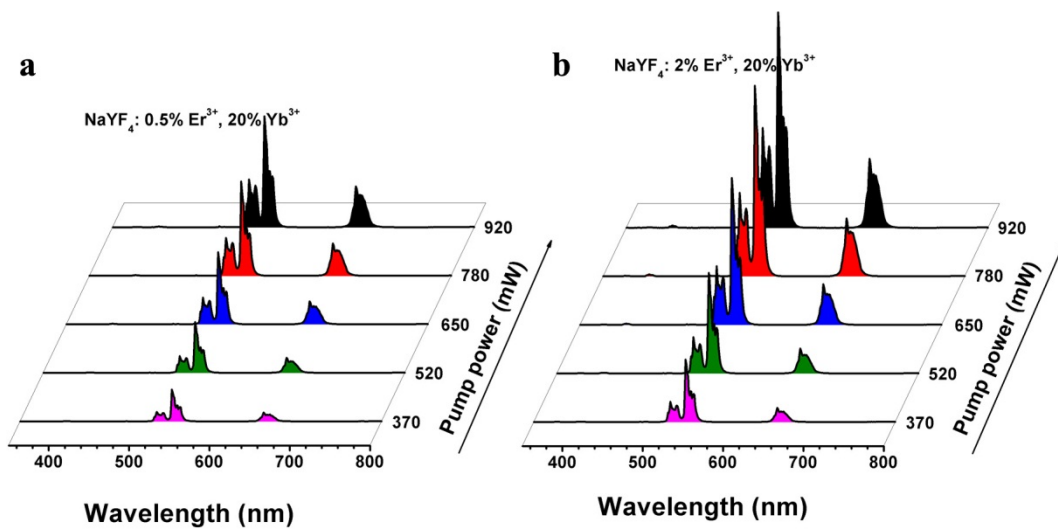


Figure S9. Pump-power-dependent UC emission spectra of (a) $\text{NaYF}_4: 0.5\% \text{Er}^{3+}, 20\% \text{Yb}^{3+}$ and (b) $\text{NaYF}_4: 2\% \text{Er}^{3+}, 20\% \text{Yb}^{3+}$ micro-crystals.

6. Biocompatibility of $\text{Lu}_5\text{O}_4\text{F}_7: \text{Er}^{3+}, \text{Yb}^{3+}$ nanoparticles

The biocompatibility of as-prepared $\text{Lu}_5\text{O}_4\text{F}_7: \text{Er}^{3+}, \text{Yb}^{3+}$ nanoparticles was investigated. Figure S10 exhibits the viability of HeLa cells treated with different concentration of the nanoparticles for 24h, tested by MTT assay. By coculturing with $\text{Lu}_5\text{O}_4\text{F}_7: \text{Er}^{3+}, \text{Yb}^{3+}$ nanoparticles at concentrations of 200 and 400 $\mu\text{g/mL}$, the cellular viability maintains around 90%. When the concentration is increased to 800 $\mu\text{g/mL}$, the cellular viability is still over 80%. These results suggest that the $\text{Lu}_5\text{O}_4\text{F}_7: \text{Er}^{3+}, \text{Yb}^{3+}$ upconversion nanoparticles possess low cytotoxicity and good biocompatibility.

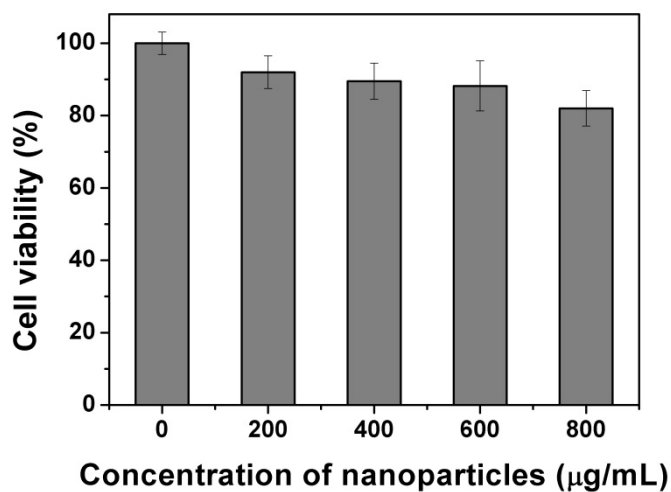


Figure S10. Cell viability of HeLa cells treated with different concentration of $\text{Lu}_5\text{O}_4\text{F}_7: \text{Er}^{3+}, \text{Yb}^{3+}$ upconversion nanoparticles.

References

- 1 J.-H. Müller, T. Petzel and B. Hormann, *Thermochimica acta*, 1997, **298**, 109-114.
- 2 W. Luo, Y. Wang, Y. Chen, T. Wen, M. Liu, Y. Wang, F. Liao and J. Lin, *J. Mater. Chem. C*, 2013, **1**, 5711-5717.
- 3 X. Zhai, J. Li, S. Liu, X. Liu, D. Zhao, F. Wang, D. Zhang, G. Qin and W. Qin, *Opt. Mater. Express*, 2013, **3**, 270-277.
- 4 W. Chen, J.-O. Bovin, A. G. Joly, S. Wang, F. Su and G. Li, *The Journal of Physical Chemistry B*, 2004, **108**, 11927-11934.
- 5 Y. Sun, Y. Chen, L. Tian, Y. Yu, X. Kong, J. Zhao and H. Zhang, *Nanotechnology*, 2007, **18**, 275609.